Radiography 31 (2025) 102958

Contents lists available at ScienceDirect

Radiography

journal homepage: www.elsevier.com/locate/radi

Reduction of radiation exposure in chest radiography using deep learning-based noise reduction processing: A phantom and retrospective clinical study

K. Mori [a, b, *], T. Negishi [b], R. Sekiguchi [a], M. Suzaki [a]

[a] Department of Radiological Technology, Saiseikai Kawaguchi General Hospital, 5-11-5 Nishikawaguchi, Kawaguchi, Saitama, 332-8558, Japan
[b] Department of Radiological Sciences, Graduate School of Human Health Sciences, Tokyo Metropolitan University, 7-2-10 Higashi-Ogu, Arakawa, Tokyo, 116-8551, Japan

ARTICLE INFO

Article history:
Received 18 December 2024
Received in revised form
2 April 2025
Accepted 7 April 2025
Available online 24 April 2025

Keywords:
Deep learning-based noise reduction
Chest X-ray imaging optimization
Radiation dose reduction
Image quality assessment

ABSTRACT

Introduction: Intelligent noise reduction (INR), a deep learning-based noise reduction developed by Canon, is used in planar radiography to improve image quality and reduce patient exposure dose. This study aimed to evaluate the reduction of patient exposure dose in planar chest radiography using INR.
Methods: We evaluated the visibility of a Lungman phantom with tumor inserts by mean opinion score (MOS) to evaluate the optimal imaging conditions for INR. Furthermore, the optimal imaging conditions for INR were verified through retrospective evaluation using clinical images and the image quality was evaluated by blind/referenceless image spatial quality evaluator (BRISQUE). The individuals were the same 100 patients who had planar chest X-rays taken without INR and with INR, designated as the control and evaluation groups, respectively. Imaging conditions with automatic exposure control in the evaluation group set the radiation dose 32 % lower than that for the control group. The BRISQUE and entrance surface dose ($K_{a,e}$) in each group were compared.
Results: Regarding the visibility of the simulated mass, there was no significant difference in MOS when the reference dose was reduced by 33.33 % ($p = 0.26$). In retrospective evaluation of clinical images, BRISQUE in the control and evaluation groups was 34.35 ± 4.19 and 34.46 ± 4.58 ($p = 0.35$), respectively. The $K_{a,e}$ in the control and evaluation groups were 0.131 ± 0.039 and 0.084 ± 0.024 mGy ($p < 0.001$).
Conclusion: INR reduced patient exposure dose by an average of 35 % without decreasing image quality.
Implications for practice: These results indicate that INR can contribute to the reduction of patient radiation dose during chest radiography. The widespread use of this technology may reduce dose indices, including diagnostic reference levels.

Introduction

Owing to the development of various types of imaging diagnostic equipment as well as improvements in medical technology, patient exposure doses from imaging diagnostics and treatments using radiation are on the rise,[1] raising regional concerns. The International Commission on Radiological Protection (ICRP) has proposed diagnostic reference levels (DRLs) to optimize medical radiation,[2] which are used across various countries and regions. Roch et al. reported that the spread of flat panel detectors reduced the 75th percentile value of the dose area product in chest radiography by 27.4 %.[3] Therefore, the widespread use of new technology has the potential to considerably reduce patient exposure doses.

Recent advances in science and technology have led to efforts to apply artificial intelligence (AI) in medical imaging. The range of AI applications in medical imaging is broad and includes lesion detection,[4] survival time prediction,[5] and image quality improvement.[6] One notable application is deep learning for noise reduction, which is included in various image diagnostic equipment and used

Abbreviations: AEC, automatic exposure control; AI, artificial intelligence; BRISQUE, blind/referenceless image spatial quality evaluator; CNN, convolutional neural network; cnvNR, conventional noise reduction; CT, computed tomography; DRL, diagnostic reference level; ICRP, International Commission on Radiological Protection; INR, intelligent noise reduction; MOS, mean opinion score; MRI, magnetic resonance imaging; MTF, modulation transfer function; PET, positron emission tomography; SID, source-to-image receptor distance.

* Corresponding author. Department of Radiological Sciences, Graduate School of Human Health Sciences, Tokyo Metropolitan University, 7-2-10 Higashi-Ogu, Arakawa, Tokyo, 116-8551, Japan.
E-mail address: mori-kazuya@ed.tmu.ac.jp (K. Mori).

https://doi.org/10.1016/j.radi.2025.102958

in clinical settings. Additionally, in positron emission tomography and magnetic resonance imaging, the usefulness of improving image quality through noise reduction processing using deep learning has been reported.[7,8] In computed tomography (CT), deep learning-based image reconstruction has been shown to reduce radiation exposure by approximately 48 % compared to hybrid iterative reconstruction,[9] and by more than 50 % compared to filtered back projection.[10] For planar X-ray imaging, intelligent noise reduction (INR), a noise-reduction process that uses deep learning, has been developed and is now used in clinical settings. INR is a deep learning-based noise reduction process developed by Canon that uses a large number of clinical images as training data to enable significant noise improvement without reducing the resolution characteristics of the image. Only vendors are allowed to select and add training data, while users can change the intensity of noise reduction processing using ten different levels.[11]

In the physical evaluation, no loss of modulation transfer function (MTF) was observed when the MTF of INR was compared with that of the original image.[11] Furthermore, in conventional noise reduction (cnvNR), the removed noise components include some signals that constitute the image. However, INR has been reported to alleviate this problem.[11] In a study presenting clinical use of INR, Hussner et al. reported the possibility of reducing patient exposure dose with INR in adult plain pelvic radiography.[12] However, few studies have evaluated the image quality of clinical planar X-ray images of adults using INR, and the optimization of the imaging dose has not been adequately verified. This study aimed to determine the optimal imaging conditions for chest X-ray imaging using deep learning-based noise reduction and to evaluate the reduction rate of patient radiation dose by noise reduction processing based on deep learning.

Method

INR uses Canon's original convolutional neural network (CNN) optimized for the detector. By optimizing the number of calculations while maintaining network complexity, images can be processed in a shorter time interval while delivering higher performances. Fig. 1 shows the image processing process of the INR.

Equipment and materials

Images were acquired using an indirect flat panel detector CXDI-410C (Canon Medical Systems, Japan), X-ray tube equipment DRX-3724HD (Canon Medical Systems), X-ray generator KXO-80SS (Canon Medical Systems), an anti-scatter grid MS X-RAY GRID (Mitaya Manufacturing, Japan), and a chest phantom N-1 LUNGMAN (Kyoto Kagaku, Japan). The anti-scatter grid had a focusing distance of 180 cm, grid density of 52 lines/cm, grid ratio of 10:1, and an intermediate aluminum material. The entrance surface dose was measured using an electrometer EMF521A (EMF, Japan) and an ionization chamber dosimeter (DC300 type, 3 cm^3 fingertip type; IBA Dosimetry, Germany). We used RadiForce GS521 (EIZO, Japan)—a 5 MP medical image display monitor—for the subjective evaluation. Python 3.12 was used to build the system for performing no-reference image quality assessment of clinical images.

Verification of imaging conditions using phantom images

Acquisition of evaluation images

We verified whether the INR imaging conditions used in clinical practice were appropriate by using phantom images containing simulated tumors. The imaging conditions for obtaining phantom images were determined by planar chest X-ray imaging. The reference image was a chest phantom acquired using cnvNR with default automatic exposure control (AEC) settings. A chest phantom image with a cnvNR effect of 10 obtained under the imaging conditions of a tube voltage of 125 kV, tube current of 200 mA, tube current−time product of 2.4 mAs, and source-to-image receptor distance (SID) of 200 cm was used as the reference image. The chest phantom contained simulated tumors 10 mm in diameter with a CT value of +100 in the lung field and mediastinum. Chest phantom images with an INR effect of 10 obtained under the tube current−time product of 0.8 mAs, 1.2 mAs, 1.6 mAs, and 2.0 mAs were used as the evaluation images. The simulated tumors in each evaluation image were at a fixed position. The reference value for the tube current time product was 2.4 mAs (i.e., dose reduction rate 0 %). The evaluation images were reduced in steps of 0.4 mAs, reducing the radiation dose by a maximum of 66.7 %. Fig. 2 shows a planar chest radiograph of the simulated tumor. Table 1 shows the image acquisition conditions used for the tumor evaluation.

Subjective evaluation

For the subjective evaluation, the confidence rating method was used to evaluate the visibility of tumors on planar chest images. The visual evaluation was performed on the five acquired phantom images. The evaluators received training in advance to ensure the uniformity of the criteria. The simulated tumors in the lung field and mediastinum were magnified and visually evaluated. We attempted to limit repeated evaluation of images. We also defined the magnification size for observing the simulated tumor (2.00× magnification) and restricted enlarging, reducing, and changing the image contrast, image density, and other image processing. Fig. 3 shows the images used for the visual evaluation. The visibility of tumors on planar chest images was evaluated using a 5-point scale (5; excellent, 4; good, 3; fair, 2; poor, 1; bad) using the mean opinion score (MOS). Table 2 lists the evaluation criteria for MOS. The visual evaluators were 12 radiological technologists (2−22 years in charge, average ± standard deviation: 10.75 ± 6.49 years) in charge of general radiography. Significant differences between reference and evaluation image were calculated using steel's multiple comparison test with reference to the Wilcoxon rank-sum test. Statistical significance was set at $p < 0.05$.

Retrospective evaluation of clinical images

No-reference image quality assessment

We used a blind/referenceless image spatial quality evaluator (BRISQUE) for image quality assessment of clinical images. BRISQUE is based on an algorithm that mimics human visual sensations and has been reported to intuitively assess image quality.[13] For this reason, it is expected that the image quality score obtained by BRISQUE will correlate with human visual assessment. BRISQUE extracts features from images and estimates image quality based on local statistical information of the image. The algorithm evaluates image quality with a score from 0 to 100, with smaller values indicating higher image quality.[14] Since BRISQUE is an image quality assessment method based on supervised learning using a support vector machine, the mean subtracted contrast normalized to the training data and the corresponding MOS were used for training. Three hundred normal adult chest X-ray images were used as the training data for BRISQUE. The training data were planar chest X-ray images obtained during a screening test judged by two radiologists to have no lesions. The participants were 150 men and 150 women, with a mean age of 55.02 ± 16.81 years. The AEC set the imaging conditions with a tube voltage of 125 kV, SID of 200 cm, and tube current−time product of 1.2−8.2 mAs. Fig. 4 shows the flow of the BRISQUE analysis.

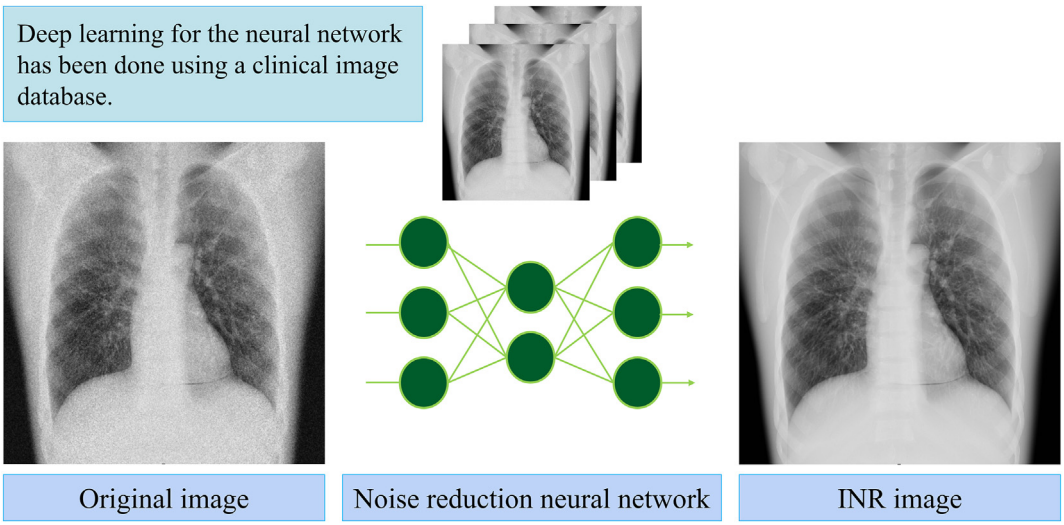

Figure 1. Process of INR image processing. INR, intelligent noise reduction.

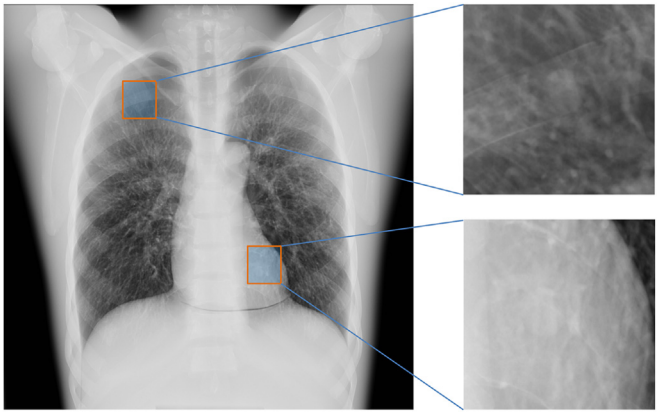

Figure 2. Planar chest radiograph of the simulated tumor.

Subject of retrospective evaluation

The optimal INR imaging conditions were verified through a retrospective evaluation of clinical images, in which the AEC setting value changed depending on INR presence or absence. This study was conducted with the approval of the ethical review board of our institution. As patient data was anonymized in this study, the institutional review board of our institution waived patient consent. The participants in the evaluation were the 100 patients (50 men and 50 women; mean age, 60.33 ± 14.02 years), who underwent planar chest radiography using cnvNR and INR from September 2023 to March 2024 and were designated as the control and evaluation groups, respectively. Inclusion criteria for this study were adult patients with a chest radiograph done using cnvNR and INR during the evaluation period. These individuals were randomly selected. Furthermore, these 100 individuals were different from the 300 patients who were part of the training data used for BRISQUE analysis. Although the individuals had a variety of lesions, images that showed changes in the patient's condition during the study period, such as disease progression or medical device insertion, were excluded from the study. The radiation dose setting using AEC can be changed in 16 % increments, and the AEC setting for the evaluation group was set to reduce the radiation dose by 32 % compared to the control group. Additionally, we have restricted the modification of these settings.

Patient radiation dose assessment

The imaging device used in this study was not equipped with a dose area product meter. Therefore, imaging conditions were retrospectively compiled from the digital imaging and communications in medicine information attached to the clinical images. The entrance surface doses ($K_{a,e}$) of the evaluation and control groups were measured using a phantom.[15] The measurement point was constant and was performed using an ionization chamber dosimeter based on the acquired imaging conditions. Fig. 5 shows the geometric arrangement for dosimetry. Significant differences in the $K_{a,e}$ between the evaluation and control groups were calculated using paired *t*-test. The $K_{a,e}$ in the chest phantom determined as follows:

$$K_{a,e} = K_{air} \times \left(\frac{SCD}{SSD}\right)^2 \times BSF \quad (1)$$

where K_{air} indicates absorbed dose corrected with correction factors, *SCD* indicates the distance from the X-ray tube focus to the chamber, *SSD* indicates the distance from the X-ray tube focus to the phantom surface, and *BSF* indicates the backscatter factor calculated from X-ray energy and X-ray field size.[16] The measurements were repeated 10 times, and the average value was used. K_{air} was corrected as follows:

Table 1
Imaging conditions for simulated tumor evaluation.

Evaluation image	0.8 mAs (INR)	1.2 mAs (INR)	1.6 mAs (INR)	2.0 mAs (INR)	2.4 mAs (cnvNR)
Radiation dose reduction rate (%)	66.7	50.0	33.3	16.7	0
INR	+	+	+	+	−

INR: intelligent noise reduction, cnvNR: conventional noise reduction.

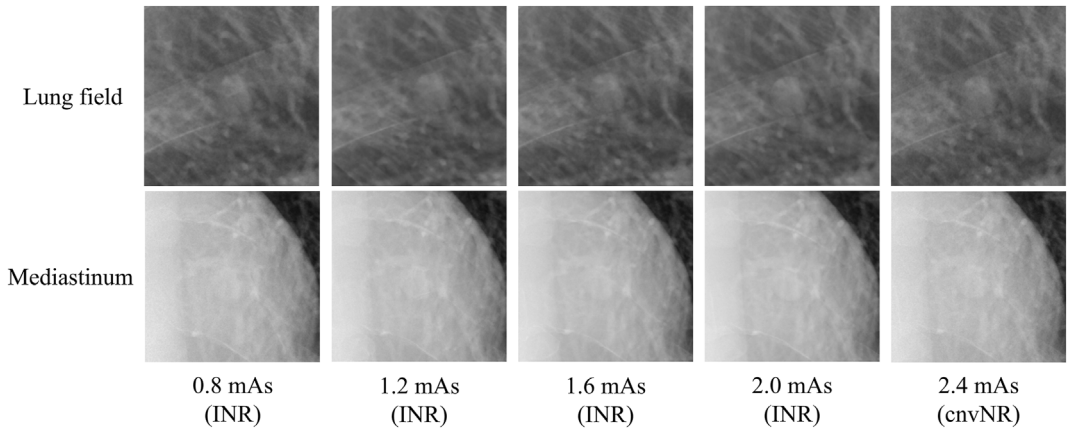

Figure 3. Simulated tumor images for visual evaluation. INR, intelligent noise reduction; cnvNR, conventional noise reduction.

Table 2
MOS used for visibility of simulated tumor.

MOS (visibility of simulated tumor)		
5	Excellent	Clear
4	Good	Somewhat clear
3	Fair	Slightly unclear but observable
2	Poor	Unclear and difficult to observe
1	Bad	Not observable

MOS: mean opinion score.

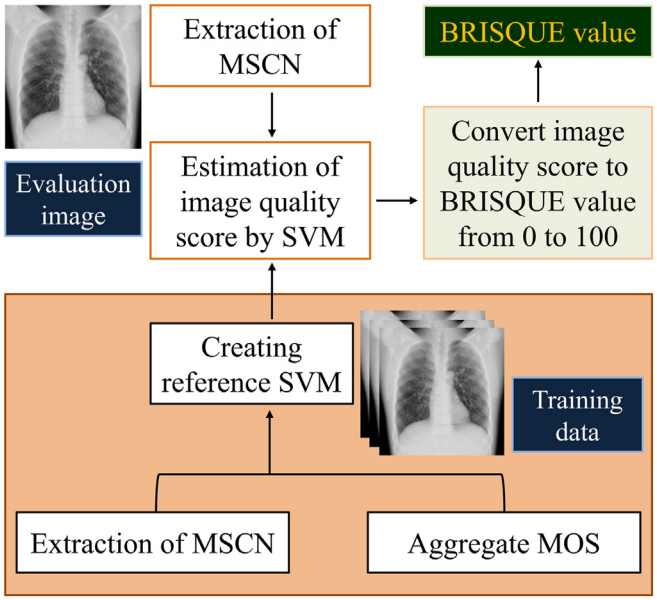

Figure 4. Flow of the BRISQUE analysis. BRISQUE, blind/referenceless image spatial quality evaluator; SVM, support vector machine; MSCN, mean subtracted contrast normalized; MOS, mean opinion score.

$$K_{air} = \overline{K}_{air} \times k_{TP} \quad (2)$$

where $\overline{K}_{air}$ indicates display absorbed dose, K_{TP} indicates temperature and pressure correction coefficient.

Image quality assessment

The quality of planar chest radiographs from the control and evaluation groups was evaluated using BRISQUE. Significant differences between evaluation and control groups were calculated using paired *t*-test.

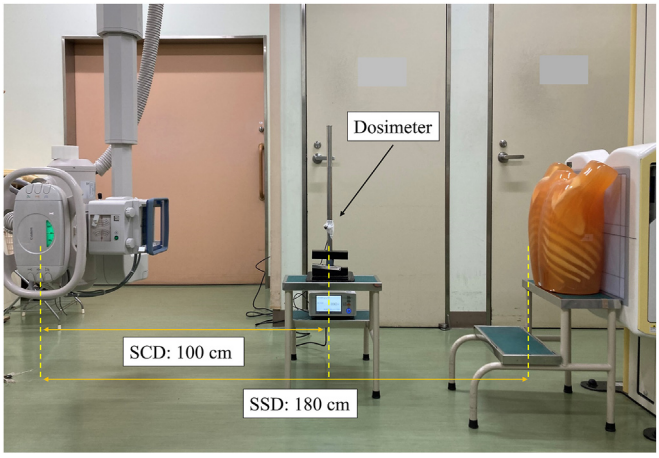

Figure 5. Geometric arrangement for dosimetry. SCD, source-to-chamber distance; SSD, source-to-surface distance.

Results

Fig. 6 shows the MOS for visibility evaluation of tumors in the lung field, whereas Fig. 7 shows the MOS for visibility evaluation of tumors in the mediastinum. When the radiation dose for chest images using INR was reduced by 50 % compared to the cnvNR images, the MOS for tumor visibility decreased significantly ($p = 0.024$). Conversely, a 33 % reduction in radiation dose using INR did not result in a significant difference in MOS for tumor visibility ($p = 0.26$).

Fig. 8 shows the evaluation of BRISQUE in the clinical images. The BRISQUE of the control and evaluation groups were 34.35 ± 4.19 and 34.46 ± 4.58 ($p = 0.35$), respectively. The BSF used for the $K_{a,e}$ measurement was 1.54. Fig. 9 shows the evaluation of $K_{a,e}$ in the clinical images. The $K_{a,e}$ of the control and evaluation groups were 0.131 ± 0.039 mGy and 0.084 ± 0.024 mGy, respectively, and the $K_{a,e}$ was significantly reduced by using INR ($p < 0.001$).

Discussion

In the visibility evaluation of phantom images, no significant difference in the visibility of the simulated tumor in the lung field

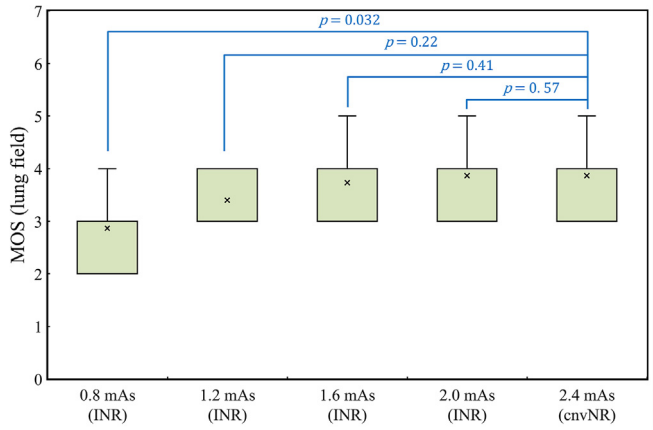

Figure 6. MOS for visibility evaluation of tumors in the lung field. MOS, mean opinion score; INR, intelligent noise reduction; cnvNR, conventional noise reduction.

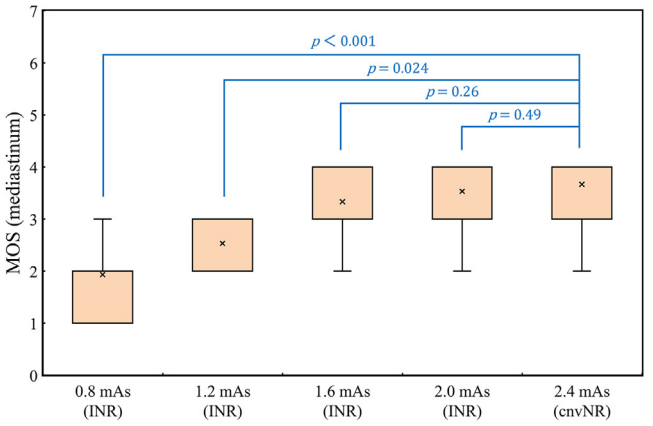

Figure 7. MOS for visibility evaluation of tumors in the mediastinum. MOS, mean opinion score; INR, intelligent noise reduction; cnvNR, conventional noise reduction.

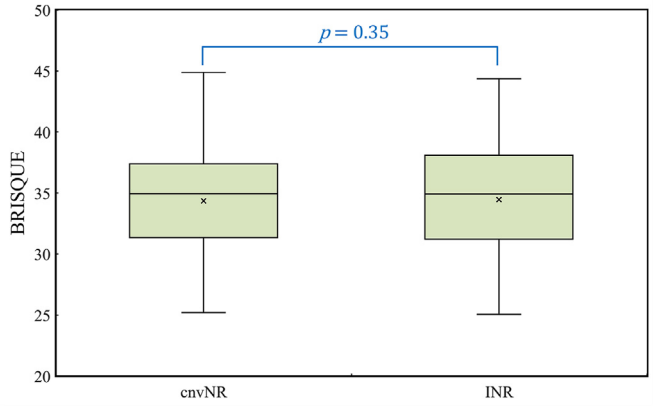

Figure 8. Evaluation of BRISQUE in the clinical images. BRISQUE, blind/referenceless image spatial quality evaluator; INR, intelligent noise reduction; cnvNR, conventional noise reduction.

was observed between the INR image with 50 % reduction in the radiation dose and the cnvNR image under standard imaging conditions. However, in the mediastinum, where noise was noticeable, unclear structure was observed in the simulated tumor in the INR image obtained by reducing the radiation dose by 50 % from the

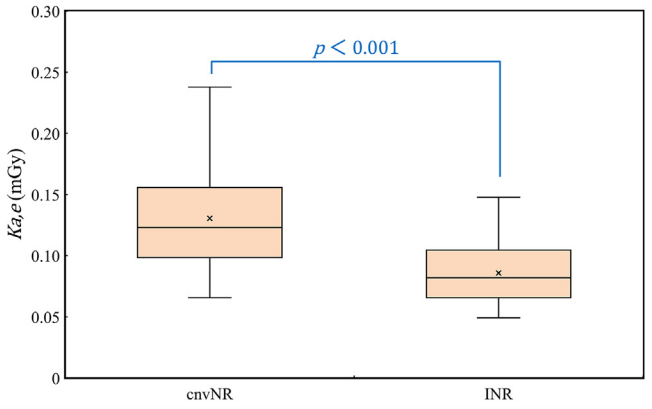

Figure 9. Evaluation of $K_{a,e}$ in the clinical images. $K_{a,e}$, entrance surface dose; INR, intelligent noise reduction; cnvNR, conventional noise reduction.

standard imaging conditions, and visibility was significantly reduced. It was suggested that it was difficult to restore the original structure even using INR in images with too much noise. The simulated tumor in the INR image, which was reduced by 33.33 % from the reference dose, did not show a significant difference in MOS. The AEC setting could be changed in 16 % increments of irradiation time. Therefore, the imaging conditions in which the AEC setting value was reduced by 32 % from that in standard imaging conditions were considered appropriate for INR.

We used BRISQUE for the retrospective image quality evaluation of clinical images. No significant difference was found between cnvNR and BRISQUE assessments for planar chest X-ray images using INR in the retrospective image quality evaluation of clinical images. The average $K_{a,e}$ for chest X-ray using INR was approximately 35 % lower than the $K_{a,e}$ of chest X-ray using cnvNR, and patient radiation dose was significantly reduced. Moreover, ICRP Publication 135 recommends optimizing the imaging dose for each modality in each country and region using DRLs.[17] The target of the current study was Japan; in Japan, Japan DRLs 2020 is used, and the DRL value of chest X-ray is set as $K_{a,e}$ at 0.30 mGy.[18] The median $K_{a,e}$ of chest X-ray using INR was 0.084 mGy, suggesting that by using INR, it is possible to acquire chest X-ray images at a dose of approximately 28 % of the DRL value defined by Japan DRLs without degrading the image quality. The CNN used in INR is trained to remove noise by considering the frequency characteristics of noise at all dose levels and reproducing the frequency characteristics of noise with tens of millions of input patterns.[11] INR makes it possible to reduce the noise without reducing the signal in the structures. Therefore, in the quality evaluation of clinical images, image quality was maintained even when the radiation dose was reduced. Chest X-ray is reported to be the most frequently performed X-ray examination in many countries.[19] Additionally, given that chest X-ray affects multiple organs with high radiation sensitivity, the reduction of patient radiation dose during chest X-ray using INR is a notable contribution to medical care.

Among the limitations of this study is the use of INR: a deep learning-based noise reduction technology manufactured by Canon. INR uses a large number of clinical images set by the vendor as training data to reduce noise in the images. Therefore, increasing the number and variety of training data may enable further reduction of noise as well as a reduction in patient radiation dose. Furthermore, this study was limited to adult planar chest X-ray images. Future studies should explore whether similar dose reductions can be achieved in other imaging regions and verify the appropriateness of radiation dose reduction for the different clinical imaging conditions of each imaging site.

Conclusion

The study identified the optimal imaging conditions for planar chest X-ray imaging using deep learning-based noise reduction. This technique maintains the same visibility as conventional noise reduction processing and can reduce patient radiation exposure dose by an average of 35 %. Noise reduction processing based on deep learning enables planar chest X-ray imaging at a dose of approximately 28 % of the DRL value defined by the Japanese DRLs.

Informed consent

As a retrospective study, the institutional review board approval was obtained without requiring patient informed consent.

Ethical approval

All procedures involving human participants were performed in in accordance with the ethical standards of the Institutional Review Board and with the 1964 Helsinki declaration and its later amendments or comparable ethical standards. This study was conducted as a retrospective, observational study and approved by the Institutional Review Board of Saiseikai Kawaguchi General Hospital (Approval Number: 2023-52) and Tokyo Metropolitan University (Approval Number: 24021).

Data availability statement

The data that support the findings of this study are not openly available due to reasons of sensitivity but are available from the corresponding author upon reasonable request. Data are stored in controlled access data storage system at Saiseikai Kawaguchi General Hospital.

Conflict of interest statement

None.

Acknowledgments

The authors would like to thank Editage (http://www.editage.com) for editing this manuscript for English language. This research did not receive any specific grant from funding agencies in the public, commercial, or not-for-profit sectors.

References

1. Mettler FA Jr, Bhargavan M, Faulkner K, Gilley DB, Gray JE, Ibbott GS, et al. Radiologic and nuclear medicine studies in the United States and worldwide: frequency, radiation dose, and comparison with other radiation sources-1950-2007. *Radiology* 2009;**253**:520–31.
2. International Commission on Radiological Protection. Radiological protection and safety in medicine. ICRP publication 73. Ann ICRP 26 (2).
3. Roch P, Célier D, Dessaud C, Etard C, Rehani MM. Long-term experience and analysis of data on diagnostic reference levels: the good, the bad, and the ugly. *Eur Radiol* 2020;**30**:1127–36.
4. Ueda D, Yamamoto A, Nishimori M, Shimono T, Doishita S, Shimazaki A, et al. Deep learning for MR angiography: automated detection of cerebral aneurysms. *Radiology* 2019;**290**:187–94.
5. Zhang K, Zuo W, Chen Y, Meng D, Zhang L. Beyond a Gaussian denoiser: residual learning of deep CNN for image denoising. *IEEE Trans Image Process* 2017;**26**:3142–55.
6. Huang L, Chen J, Hu W, Xu X, Liu D, Wen J, et al. Assessment of a radiomic signature developed in a general NSCLC cohort for predicting overall survival of ALK-positive patients with different treatment types. *Clin Lung Cancer* 2019;**20**:63851.
7. Bonardel G, Dupont A, Decazes P, Queneau M, Modzelewski R, Coulot J, et al. Clinical and phantom validation of a deep learning based denoising algorithm for F-18-FDG PET images from lower detection counting in comparison with the standard acquisition. *EJNMMI Phys* 2023;**9**:36.
8. Feuerriegel GC, Weiss K, Kronthaler S, Leonhardt Y, Neumann J, Wurm M, et al. Evaluation of a deep learning-based reconstruction method for denoising and image enhancement of shoulder MRI in patients with shoulder pain. *Eur Radiol* 2023;**33**:4875–84.
9. Zhang Q, Lin Y, Zhang H, Ding J, Pan J, Zhang S. The application value of a vendor-specific deep learning image reconstruction algorithm in "triple low" head and neck computed tomography angiography. *Quant Imaging Med Surg* 2024;**14**:2955–67.
10. Koetzier LR, Mastrodicasa D, Szczykutowicz TP, van der Werf NR, Wang AS, Sandfort V, et al. Deep learning image reconstruction for CT: technical principles and clinical prospects. *Radiology* 2023;**306**:e221257.
11. Johnson J. Intelligent noise reduction: seeing through the noise with deep learning image processing. *Canon Technical White Paper*. 2023:1–18. https://mcu.canon/downloads_canon_com/cmcu/pdfs/Intelligent_NR_Technical_White_Paper.pdf. [Accessed 25 September 2024].
12. Hussner ED, Sundby S, Outzen CB, Jensen J, Tingberg A, Precht H. How does intelligent noise reduction software influence the image quality in pelvic digital radiography; a phantom study. *J Med Imag Radiat Sci* 2025;**56**:101814.
13. Fang Y, Ma K, Wang Z, Lin W, Fang Z, Zhai G. No-reference quality assessment of contrast-distorted images based on natural scene statistics. *IEEE Signal Process Lett* 2015;**22**:838–42.
14. Anish M, Anush KM, Alan CB. No-reference image quality assessment in the spatial domain. *IEEE Trans Image Process* 2012;**21**:4695. -08.
15. International commission on radiation units and measurements. Patient Dosimetry for X-Rays used in Medical Imaging. ICRU Report: 74.
16. Kato H. Method of calculating the backscatter factor for diagnostic X-rays using the differential backscatter factor. *Nippon Hoshasen Gijutsu Gakkai Zasshi* 2001;**57**:1503–10.
17. International Commission on Radiological Protection. Diagnostic reference levels in medical imaging. *Ann ICRP* 2017;**46**. ICRP Publication;1:135.
18. *Japan network for research and information on medical exposure. Natl Diagn Ref Levels Jpn. 2020 - Japan DRLs 2020*. 2020. https://j-rime.qst.go.jp/report/DRL2020_Engver.pdf. [Accessed 5 November 2024].
19. European Commission. European guidance on estimating population doses from medical X-ray procedures. *Radiat Prot* 2008;**154**. https://op.europa.eu/en/publication-detail/-/publication/72d806a2-2fb4-4e4d-a845-3b276feed8eb. [Accessed 1 December 2024].